Arab J Sci Eng (2017) 42:5031–5044
DOI 10.1007/s13369-017-2545-8

RESEARCH ARTICLE - ELECTRICAL ENGINEERING

High Impedance Fault Localization Using Discrete Wavelet Transform for Single Line to Ground Fault

Mohd Syukri Ali[1] · Ab Halim Abu Bakar[1] · ChiaKwang Tan[1] · Hamzah Arof[2] · Hazlie Mokhlis[1,2] · Mohamad Sofian Abu Talip[2]

Received: 16 February 2015 / Accepted: 11 April 2017 / Published online: 26 April 2017

Abstract This paper presents a new approach to determine the high impedance fault location in a distribution network using discrete wavelet transform (DWT). The technique comprises three stages which are fault impedance identification, faulty section localization and fault distance estimation. First, the transient voltage and current waveforms are analyzed using DWT to obtain the energy values of its coefficients. Then artificial neural network is utilized to predict the fault impedance value. Next, the database and trigonometry techniques are used to localize the faulty section and fault distance successively. The proposed method is used to detect single line to ground faults on a 38-node distribution simulated network created using the PSCAD/EMTDC software. The output waveforms are analyzed using MATLAB. The fault impedance and fault distance can be estimated with errors of less than 0.42 and 2.37%, respectively, while the faulty section can be determined within the 6th rank. The encouraging results show that the approach is capable of determining the fault impedance value, localizing the faulty section and estimating the fault distance under various fault inception angles, fault impedances and fault distances.

Keywords High impedance fault location · Discrete wavelet transforms · Artificial neural network · Distribution network

✉ Mohd Syukri Ali
mosba86@yahoo.com.my

[1] UM Power Energy Dedicated Advanced Centre (UMPEDAC), Level 4, Wisma R&D UM, Jalan Pantai Baharu, University of Malaya, 59990 Kuala Lumpur, Malaysia

[2] Department of Electrical Engineering, Faculty of Engineering, University of Malaya, 50603 Kuala Lumpur, Malaysia

1 Introduction

A typical distribution network consists of several feeders and a number of lateral branches. Due to the complex topology of the system, it is difficult to localize a fault that occurs in the network. Therefore, a reliable and accurate method that can identify the fault impedance, and location is essential, especially during the high impedance fault (HIF) event. Causes of faults are numerous. For instance, in an overhead distribution network, common causes of the faults are lightning, breakdown of line, tree limbs touching the lines and animal encroachment. In an underground network, faults are normally attributed to cable insulation deterioration and water-treeing phenomena [1].

Locating a fault in an underground system is challenging as the fault cannot be spotted visually [2]. Therefore, several techniques have been proposed to locate faults in an underground system and they can be grouped into three main categories. They are impedance-based techniques, traveling wave methods and expert systems [1,3–15]. In [1,14,15]. Fault localizations based on impedance-based techniques require the voltage and current signals to be measured at the main substation during fault to generate multiple possible fault locations. Besides, they cannot detect HIF events because the measured voltage and current signals are very similar to the nominal values.

Fault localization using traveling wave technique that can determine the fault distance in a transmission system was proposed by Elhaffar [6]. However, this method is not suitable for a distribution system with many lateral branches due to multiple reflections of the injected signal coming from the fault point and tee-connection in the network. A number of updated works that use this method have been reported in [3,7,9,16]. In [8], a method based on path characteristic frequency (PCF) using traveling wave signal is proposed.

Expert systems have also been used to locate faults in a distribution network. ANN [5,8,13,17], support vector regression (SVR) [9] and fuzzy logic system (FLS) [11] have been employed to estimate the fault distance and fault location in a radial distribution system. For more accurate prediction of the fault distance, a hybrid of two or more expert systems has been proposed. For instance, a combination of ANN and SVR [4] and ANN and FLS [10] has been used to determine the type and location of faults. Recently, a new expert system called core vector regression (CVR) [12] has been used for locating faults in a large distribution network.

An expert system must be trained well with a good set of features extracted from samples of voltage and current signals. To obtain good features, a suitable feature extractor like wavelet transform (WT) [7–10,18–20] can be used. WT has the capability to decompose a signal into high- and low-frequency components which are useful for analyzing the transient signals during fault. A new feature extractor called Empirical Mode Decomposition (EMD) was proposed in [12]. Several other methods have also been proposed for fault location detection in overhead distribution systems [21,22]. Nam et. al. [21] utilized the absolute difference of approximate zero-sequence angles between two adjacent nodes to locate faults. The fault distance was calculated using the synchronized zero-sequence voltage and current signals at the faulted node. Xiu and Liao [22] introduced an approach that estimates the location of the fault based on the product of bus impedance matrix and current injected at the substation. Likewise in [23], HIF locations are identified by parameter estimation approach.

It must be noted that almost all of the techniques mentioned above can only be applied for locating low impedance faults. High impedance fault localization remains a huge challenge. As such, this paper will present a new HIF localization technique which consists of 3 stages: fault impedance identification, faulty section localization and fault distance estimation. First, the distribution network is modeled using the PSCAD/EMTDC software. This software provides a real-time power system transient simulation of load flow, short circuit, dynamic, power quality, electromagnetic transient studies, etc [24]. Then, WT is used to extract the low-frequency components (approximation coefficients) of the three-phase voltage and current signals. Based on the extracted features, an ANN in MATLAB Toolbox [25] will estimate the fault impedance value. A new approach based on the minimum and maximum DWT energy values of phase-A voltage and current is used to locate the faulty section. Finally, the shortest distance (SD) calculation and trigonometry technique are employed to estimate the fault distance. In this paper, single line to ground faults (SLGF) are investigated in a typical 38 node radial distribution network. SLGF is considered because it is the most common type of fault in a distribution system. The rest of the paper is organized as follows. In Sects. 2 and 3, some basic concepts of ANN and DWT are described. Section 4 presents the proposed HIF localization method. Results and discussion are presented in Sect. 5. In Sect. 6, conclusion and future work are given.

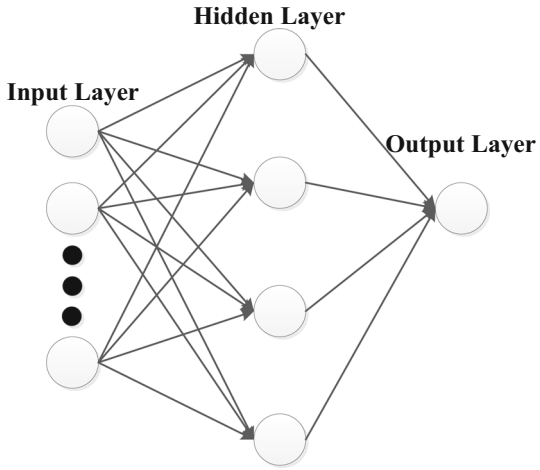

Fig. 1 Basic artificial neural network architecture

2 Artificial Neural Network (ANN)

ANN is a popular machine learning and pattern recognition classifier. It commonly consists of three layers known as the input layer, hidden layer and output layer as shown in Fig.1. Each layer has a number of nodes (or neurons) where each node in a layer is connected to all nodes in the next layer by links with weights. During training, input data are fed into the nodes of the input layer and the values of weights throughout the ANN are modified so that the expected output is obtained. There are many types of ANN depending upon their networks, topologies, learning styles, training approaches and activation functions.

The main advantage of ANN is its ease of use. It has the capability to solve random, non-linear, classification and forecasting problems. The accuracy of an ANN depends on its ability to learn the correct relationship or mapping between the input and output patterns [10].

In this work, a multi-layer feed-forward network with a sigmoid function in the hidden layer and linear function in the output layer is used. There are 6 nodes in the input layer, 6 nodes in the hidden layer and one node in the output layer. The network was trained using the Levenberg–Marquardt backpropagation algorithm to estimate the fault impedance value.

3 Discrete Wavelet Transform (DWT)

DWT is a signal processing technique which decomposes a signal $s(n)$ into low-frequency and high-frequency components as shown in Fig. 2. The low-frequency component,

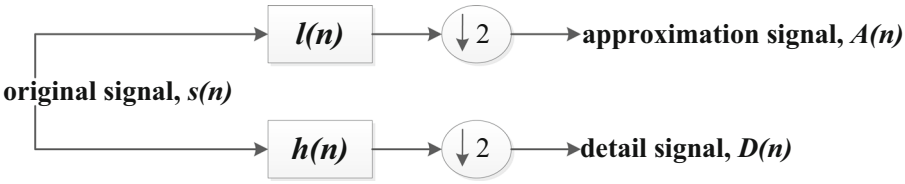

Fig. 2 Discrete wavelet transform filter analysis

also known as the *approximation signal*, is obtained when the original signal is filtered using the low-pass filter, $l(n)$ (scaling function). The high-frequency component, or the *detail signal* is produced by filtering the original signal with the high-pass filter, $h(n)$ (wavelet function) [26]. The scaling function and wavelet function can be expressed as follows:

$$l_{j,k}(n) = 2^{j/2} l(2^j n - k) \tag{1}$$

$$h_{j,k}(n) = 2^{j/2} h(2^j n - k) \tag{2}$$

where j and k represent the dilation and position parameter, respectively.

As shown in the figure, the filtering process involves downsampling operation by 2 and convolution operation. The approximation $A(n)$ and difference $D(n)$ signals can be calculated as follows:

$$A(n) = \sum s(n) * l(2n - k) \tag{3}$$

$$D(n) = \sum s(n) * h(2n - k) \tag{4}$$

The advantages of DWT over other signal processing methods such as Fourier Transform are its capability to extract important features from the signal with irregularities, discontinuities and sharp spikes.

In this paper, Daubechies wavelet level 4, Db4 is used to decompose the voltage and current waveforms during the fault event. Figure 3a shows an example of the phase-A voltage waveform with phase-A to ground fault at Node 1. The fault impedance value is 50 Ω. Figure 3b, c shows the corresponding approximation and detail coefficients. Based on the extracted detail coefficients, the time of the fault occurrence is at the position of the sharp peak as shown in Fig. 3c.

However, in order to determine the HIF fault impedance, faulty section and fault distance, only approximation coefficients are used to calculate the energy value which is obtained by summing the squared approximation coefficients over one full cycle as follows:

$$\text{EnergyValue} = \sum_{i=1}^{40} (cA\_Va)^2 \tag{5}$$

Figure 4 shows an example of the calculated energy values before and after a fault occurs within 4 full cycles of phase-A voltage.

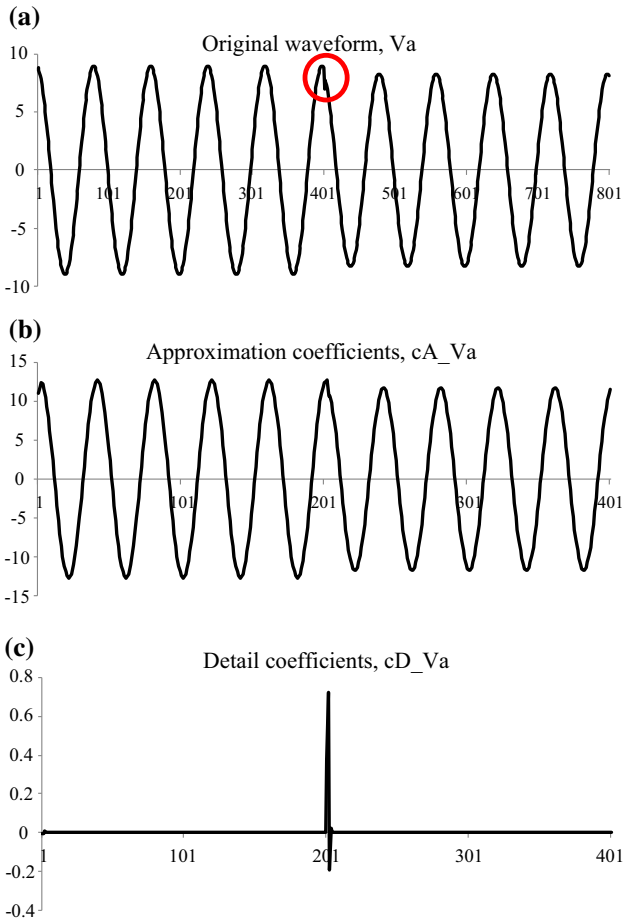

Fig. 3 Decomposition process for phase-A voltage waveform using Db4. **a** Original phase-A voltage waveform, **b** approximation coefficients of phase-A voltage waveform, **c** detail coefficients of phase-A voltage waveform

4 Proposed High Impedance Fault Localization Method

The proposed method estimates the fault impedance value, identifies the faulty section and determines the fault distance consecutively as shown in Fig. 5. Basically, the three-phase voltage and current waveforms are analyzed using DWT and the energy values of the coefficients are utilized to estimate the HIF fault impedance value. Then possible faulted sections are identified by matching the DWT energy values of the voltage and current waveforms against those stored in the database. From the comparison, possible faulty sections are

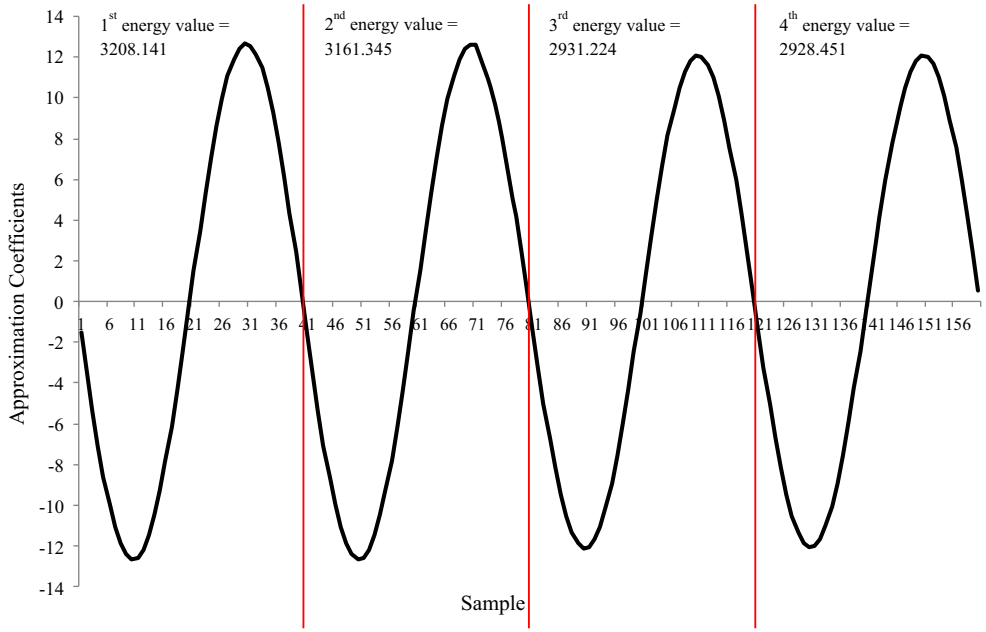

Fig. 4 Energy value

listed in ascending order using the ranking analysis method based on the shortest distance (SD) score. The most probable faulty section is the one with the smallest SD score which is ranked first. Finally, the fault distance is calculated using the trigonometry technique for the chosen faulty section.

4.1 Development of Database

As stated earlier, the proposed method utilizes a database to determine probable faulted sections. Thus, a database of voltage and current data for various fault impedance values must be developed. First, HIF of a certain impedance value is applied at each node of the network. Then the three-phase voltage and current waveforms are measured at the main substation. DWT is used to decompose the measured voltage and current before calculating the energy values. The process is repeated for different HIF values. An example of a phase-A voltage waveform obtained at the measurement point is shown in Fig. 3a. It shows the shape of the voltage cycles before and after the occurrence of a fault at cycle 5. Visually, it is difficult to spot changes in the waveform as the cycles look similar before and after the fault. This is because the voltage waveform is only slightly altered by the HIF. Figure 6 shows the profile of the faulted voltage signal compared to that of the normal one. Upon closer inspection of Fig. 3a, the starting point of the fluctuation can be observed at the peak of cycle 5, close to the 401st sample.

In the database development, a fault is initiated and the energy values of each cycle of the voltage waveforms are calculated using DWT. Figure 7 shows the energy value of the voltage cycles before and after the fault. It can be seen that after the fault occurs at cycle 3, the energy value decreases. However, in the database, only the energy value of the fifth cycle is stored as it has stabilized. The process is repeated for each node before a different HIF value is tested. The value of HIF impedance ranges from 40 to 100 Ω in increment of 10 Ω. The above steps are repeated for the current signal to establish the current database.

For instance, a fault can be triggered at node i and then j as shown in Fig. 8. The measured waveforms during the fault are analyzed and only phase-A voltage and current are processed to obtain the DWT energy values. These values are saved in the database along with the corresponding fault impedance values as shown in Table 1. The energy values of the other two phases (phase-B and phase-C) are only used as inputs to the ANN for estimating the fault impedance value but not stored in the database for faulty section localization.

Since it is impractical to test all possible fault impedance values, the fault impedance is varied by 10 Ω. Likewise, it is also not possible to measure the voltage and current at every point along a line section. Thus, for a particular section that lies between two nodes, it is best to keep only the minimum and maximum voltage and current energy values measured at the two ends (nodes) in the database as shown in Table 2. As an example, for a line section between nodes i and j, a few energy values can be calculated from the waveforms measured at nodes i and j. For 40 and 50 Ω impedances, 8 energy values can be calculated from the voltages and currents of the two nodes and they are V_{i40}, V_{i50}, V_{j40}, V_{j50}, I_{i40}, I_{i50}, I_{j40} and I_{j50} as listed in Table 1. However, if V_{i40}, V_{j50}, I_{i40} and I_{j50} represent minimum and maximum energy values of

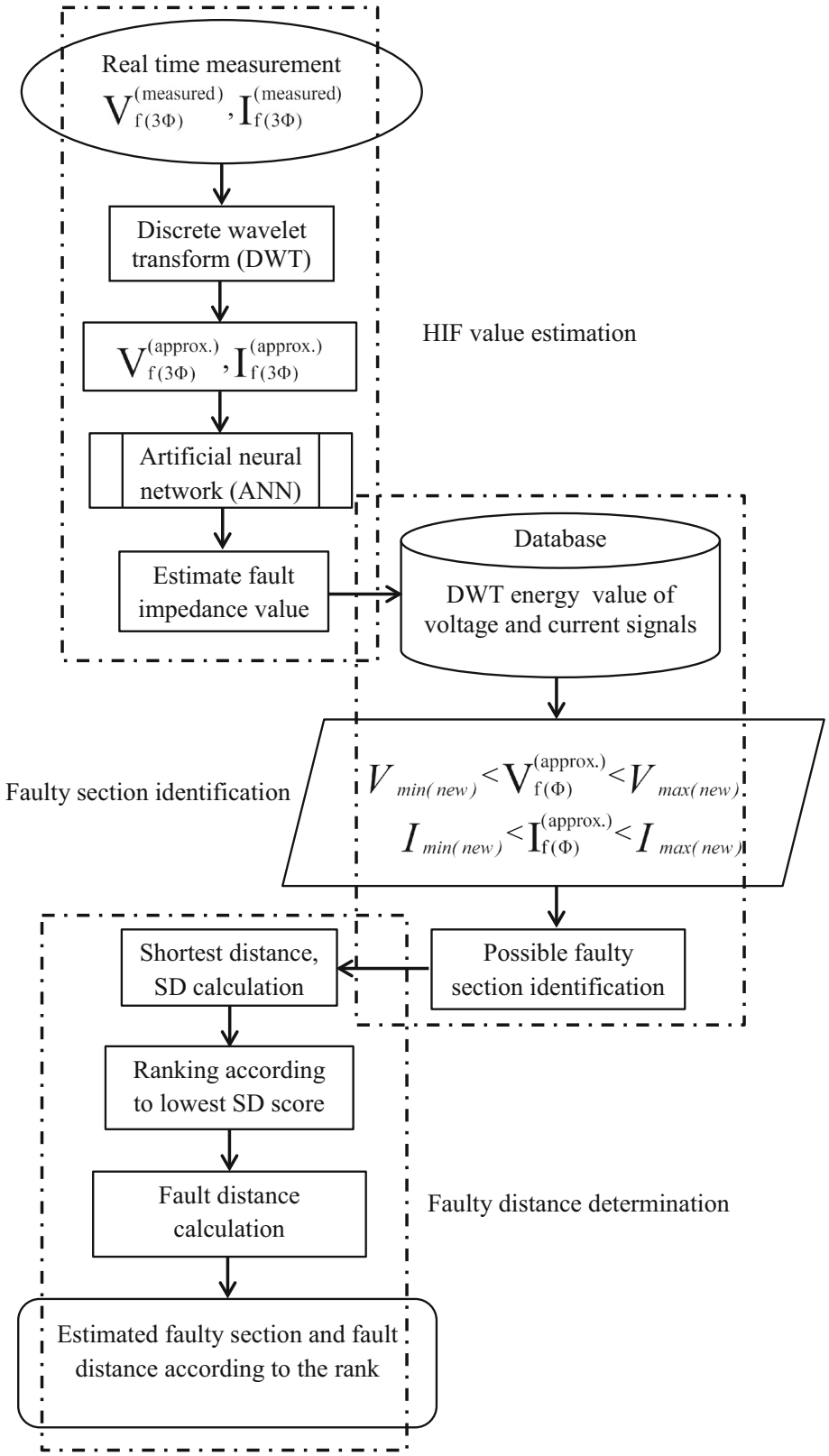

Fig. 5 Flowchart of the proposed method

the voltage and current, respectively, only they are stored in the database called Database1. The process is repeated for the other line sections and impedance intervals. The results are Database2 for 50–60 Ω interval, Database3 for 60–70 Ω interval, Database4 for 70–80 Ω interval, Database5 for 80–90 Ω interval and Database6 for 90–100 Ω interval.

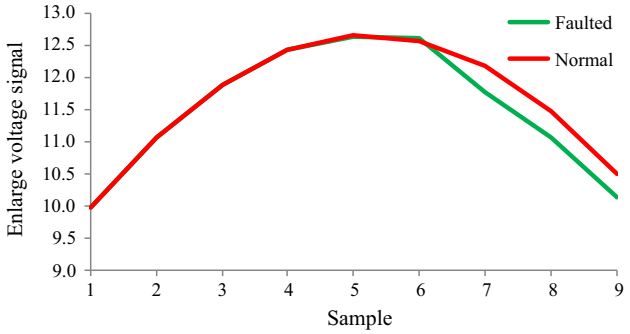

Fig. 6 Comparison between normal and faulted voltage waveforms

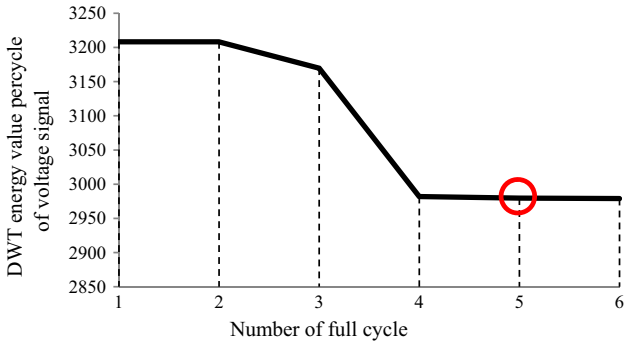

Fig. 7 Energy value of voltage signal

4.2 Fault Impedance Estimation

The fault impedance is estimated using an ANN. In the training phase, the DWT energy values of the 3-phase voltage and current waveforms at each node are fed into the ANN along with the associated impedance value. The estimated fault impedance value will assist the correct database to be selected out of the 6 databases. Based on the selected database, the possible faulty sections are determined as elaborated below.

4.3 Faulty Section Identification

The possible faulty sections are identified using the database approach which utilizes only the DWT energy values of phase-A voltage and current waveforms labeled as $V_{f(\Phi)}^{\text{approx}}$ and $I_{f(\Phi)}^{\text{approx}}$. This is done by comparing these energy values with those stored in the selected database according to Eqs. (6) and (7). If both energy values fall between the minimum and maximum stored values, the line section that generates the stored minimum and maximum values is considered faulty. The conditions are as follows:

Table 1 Energy values of voltage and current signals between 2 adjacent nodes

	40Ω	50Ω	60Ω
Node i	V_{i40} & I_{i40}	V_{i50} & I_{i50}	V_{i60} & I_{i60}
Node j	V_{j40} & I_{j40}	V_{j50} & I_{j50}	V_{j60} & I_{j60}

Table 2 Database of minimum and maximum values

	Database 1 (40–50 Ω)		Database 2 (50–60 Ω)	
	Min	Max	Min	Max
Section k	V_{i40}	V_{j50}	V_{i50}	V_{j60}
(Line section i–j)	I_{i40}	I_{j50}	I_{i50}	I_{j60}

$$V_{\text{min,section}(i)}^{\text{database(k)}} \langle V_{f(\Phi)}^{\text{approx}} \langle V_{\text{max,section(i)}}^{\text{database(k)}} \tag{6}$$

$$I_{\text{min,section}(i)}^{\text{database(k)}} \langle I_{f(\Phi)}^{\text{approx}} \langle I_{\text{max,section(i)}}^{\text{database(k)}} \tag{7}$$

where

$i = 1, 2, \ldots, 35$ (number of line section)

$k = 1, 2, \ldots, 6$ (selected database number)

To achieve a higher accuracy, the algorithm will narrow the range of energy values in the database using linear approximation method and the impedance value predicted by the ANN. The adjusted ranges of the database are compared against the calculated energy values to see within which sections the energy values fall in. For example, consider the occurrence of a fault whose impedance is estimated at 42 Ω by the ANN. The algorithm will use the 40–50 Ω database as shown in Table 2. So, the min–max ranges in the database will be adjusted according to the equations below. It is assumed that there is a ±1.5 Ω error of the impedance estimate given by the ANN such that the real value is actually within 40.5 and 43.5 Ω as shown in Fig. 9. The 40–50 Ω database is now adjusted to contain $V_{\text{min(new)}}$, $V_{\text{max(new)}}$, $I_{\text{min(new)}}$ and $I_{\text{max(new)}}$ values for the fault impedance range of 40.5–43.5 Ω. This adjusted database will then be used to identify the faulted section and fault distance.

The steps involved in the faulty section identification are outlined below:

(1) The fault impedance value is estimated using the ANN and labeled as $Z_{\text{estimated}}$.
(2) Based on the $Z_{\text{estimated}}$, the associated impedance range in the database is selected. For the above 42Ω fault impedance example, the 40–50 Ω database will be selected. Then, the linear approximation value is cal-

Fig. 8 Simplified distribution network

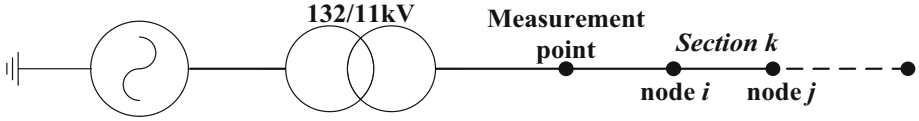

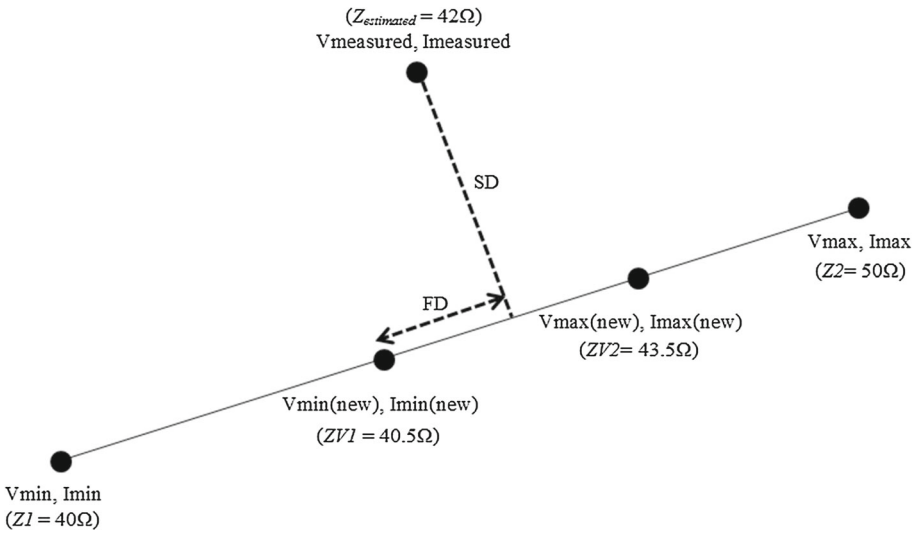

Fig. 9 An example of linear approximation technique to narrow down the impedance values in the previously established database

culated for both the voltage and current as follows:

$$\text{DiffV} = \frac{V_{\max} - V_{\min}}{10\Omega} \quad \text{DiffI} = \frac{I_{\max} - I_{\min}}{10\Omega} \tag{8}$$

(3) A new database is established in the range of $Z_{\text{estimated}} \pm 1.5\Omega$. The value of 1.5 Ω is selected after a thorough accuracies evaluation process.

$$\begin{aligned} ZV1 &= Z_{\text{estimated}} - 1.5 \\ ZV2 &= Z_{\text{estimated}} + 1.5 \\ ZV1 &< Z_{\text{estimated}} < ZV2 \end{aligned} \tag{9}$$

(4) Then, a new estimated minimum and maximum values for the voltage and current signals are obtained through the linear approximation method.

$$V_{\min(\text{new})} = V_{\min} + (ZV1 - Z1) * \text{DiffV}$$

$$V_{\max(\text{new})} = V_{\max} + (ZV2 - Z2) * \text{DiffV} \tag{10}$$

$$I_{\min(\text{new})} = I_{\min} + (ZV1 - Z1) * \text{DiffI}$$

$$I_{\max(\text{new})} = I_{\max} + (ZV2 - Z2) * \text{DiffI} \tag{11}$$

where, *Z1* and *Z2* are the lower and upper fault impedance values in the selected database. For example, in the above 40–50 Ω database, the value of *Z1* is 40 Ω while *Z2* is 50 Ω.

After obtaining the $V_{\min(\text{new})}$, $V_{\max(\text{new})}$, $I_{\min(\text{new})}$ and $I_{\max(\text{new})}$, Eqs. (6) and (7) are modified as shown in Eqs. (12) and (13). Thus, the number of possible faulty sections can be reduced.

$$V^{\text{database(k)}}_{\min(\text{new}),\text{section(i)}} < V^{\text{approx}}_{f(\Phi)} < V^{\text{database(k)}}_{\max(\text{new}),\text{section(i)}} \tag{12}$$

$$I^{\text{database(k)}}_{\min(\text{new}),\text{section(i)}} < I^{\text{approx}}_{f(\Phi)} < I^{\text{database(k)}}_{\max(\text{new}),\text{section(i)}} \tag{13}$$

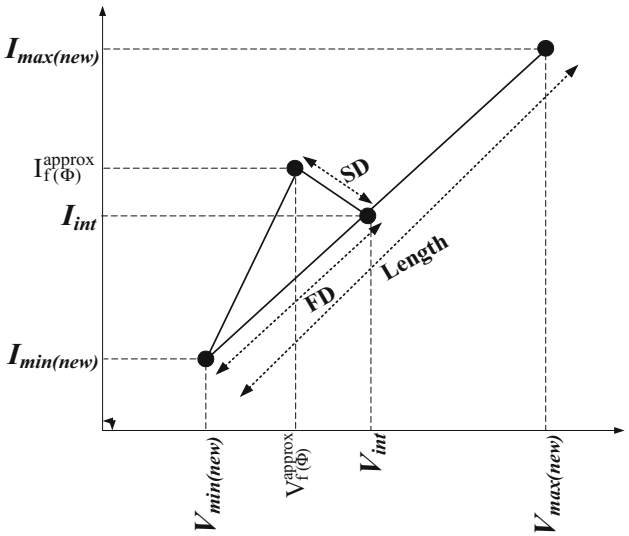

Fig. 10 Shortest distance and fault distance calculation diagram

The possible faulty section is accounted if Eqs. (12) and (13) are fulfilled. Although the number of possible faulty sections have been narrowed down, there could still exist multiple sections that can satisfy both Eqs. (12) and (13). Therefore, these possible faulty sections will be ranked from the most to the least likely based on the SD score. The SD score computations can be visualized through Fig. 10, where $V_{\min(\text{new})}$, $V_{\max(\text{new})}$, $I_{\min(\text{new})}$ and $I_{\max(\text{new})}$ are obtained from the temporary database, while $V^{\text{approx}}_{f(\Phi)}$ and $I^{\text{approx}}_{f(\Phi)}$ are the test fault data. The calculation steps for SD are as follows:

1. Find the straight line equation between ($V_{\min(\text{new})}$, $I_{\min(\text{new})}$) and ($V_{\max(\text{new})}$, $I_{\max(\text{new})}$).
2. Find the perpendicular line from (V_{approx}, I_{approx}) to straight line ($V_{\min(\text{new})}$, $I_{\min(\text{new})}$) and ($V_{\max(\text{new})}$, $I_{\max(\text{new})}$).

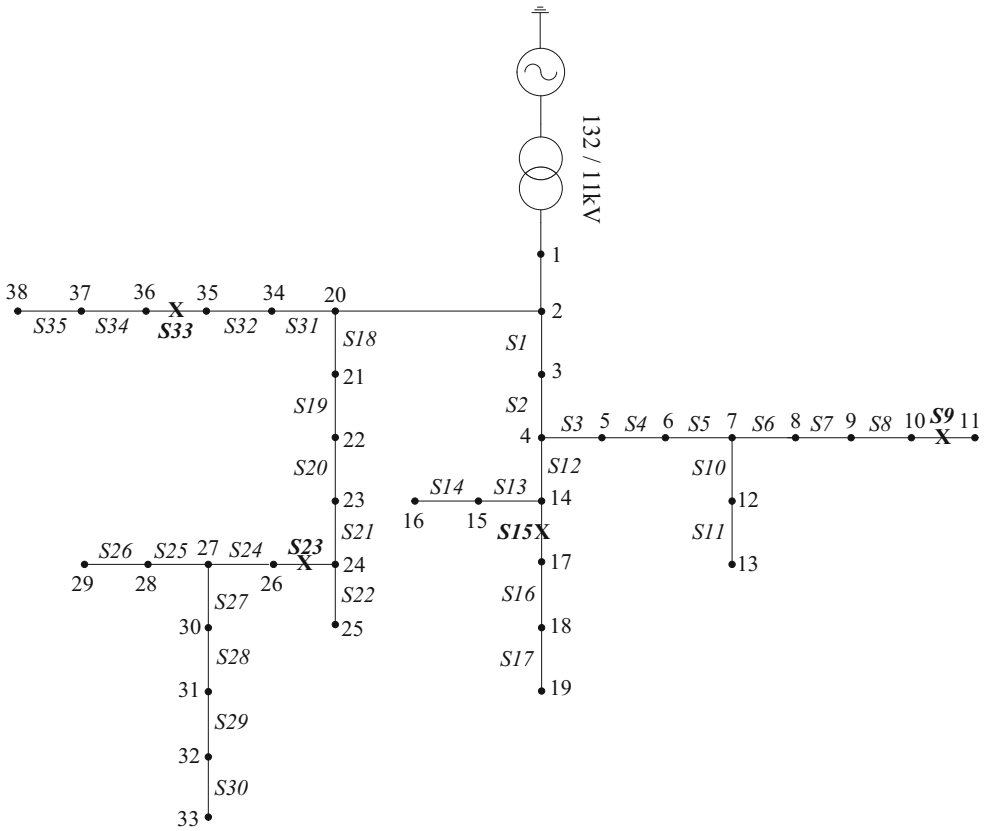

Fig. 11 38-nodes distribution network diagram

3. Find the interception point between two straight lines $(V_{\text{int}}, I_{\text{int}})$.
4. Calculate the SD score.

$$\text{SD} = \sqrt{\left(I_{f(\Phi)}^{\text{approx}} - I_{\text{int}}\right)^2 + \left(V_{f(\Phi)}^{\text{approx}} - V_{\text{int}}\right)^2} \tag{14}$$

Based on the SD score, the rank of possible faulty sections is arranged in ascending order where the section that yields the smallest SD score is ranked first. However, if the fault cannot be found in that line section, the second ranked faulty line section will be inspected and so on.

4.4 Fault Distance Estimation

In order to expedite the restoration process, it is important to estimate the fault distance in the identified faulty section, especially for the buried cable. In present practice, the surge generator is used to locate the fault in an underground distribution system. It will inject high-voltage *dc* pulse, typically up to 30 kV. However, this high-voltage thumping might jeopardize the integrity of the cable, especially for the aged cable. Thus, it is important to determine the faulty section and its distance without damaging the cable. By referring to Fig. 10, the actual fault distance can be estimated based on the formula given below:

$$\text{Actual FD} = \frac{\text{FD}}{\text{Length}} \times \text{Actual Length} \tag{15}$$

where:

FD = fault distance between $(V_{\min(\text{new})}, I_{\min(\text{new})})$ and $(V_{\text{int}}, I_{\text{int}})$.

Length = length between $(V_{\min(\text{new})}, I_{\min(\text{new})})$ and $(V_{\max(\text{new})}, I_{\max(\text{new})})$.

Actual Length = the actual length of that particular line section.

Actual FD = the actual fault distance estimation.

5 Results and Discussion

To investigate the performance of the proposed method, a single line to ground fault (SLGF) is applied in the middle of four different line sections with different fault impedance values. Only SLGF is considered in this proposed method because this type of fault commonly occurs in the distribution system. The fault is applied in the middle of line section 9, 15, 23 and 33 (marked as X) as shown in Fig. 11. The fault impedance values are 45, 65 and 85 Ω with the incep-

Table 3 Test result for fault applied in the middle of line section 9, 15, 23 and 33

45 Ω				65 Ω				85 Ω			
Section	Rank	Fault Impedance	Distance	Section	Rank	Fault Impedance	Distance	Section	Rank	Fault Impedance	Distance
(i) Fault in the middle of line section 9 (0.25 km)											
16	1	44.86	0.3045	16	1	64.98	0.2969	16	1	85.17	0.2867
14	2	44.86	0.4040	*9	2	64.98	0.3117	*9	2	85.17	0.2682
*9	3	44.86	0.3540								
(ii) Fault in the middle of line section 15 (0.25 km)											
8	1	44.87	0.1353	8	1	64.96	0.0853	11	1	84.97	0.3534
*15	2	44.87	0.3554	*15	2	64.96	0.3175	*15	2	84.97	0.3040
(iii) Fault in the middle of line section 23 (0.05 km)											
*23	1	44.37	0.0865	*23	1	64.68	0.0724	*23	1	84.63	0.0712
(iv) Fault in the middle of line section 33 (0.65 km)											
*33	1	45.39	0.7249	*33	1	65.36	0.6769	*33	1	85.46	0.6012

(*) represents the actual faulty section

tion angle of 90°. The test results of the proposed method are shown in Table 3. The first column shows the most probable faulty sections arranged based on the SD score with the smallest score ranked first. The third and fourth columns show the estimated HIF fault impedance value and fault distance, respectively.

For example, a fault is applied in the middle of line section 9 with fault impedance value of 45 Ω. Based on the DWT energy values of the voltage and current waveforms, the estimated fault impedance value is 44.86 Ω. Once the fault impedance value is determined, an appropriate database is selected to identify all the possible faulty sections using the matching approach in Eqs. (12) and (13). As shown in Table 3, the actual faulty section is located in the third rank behind the line sections 16 and 14 based on the SD score. Simultaneously, the fault distance is calculated for all possible faulty sections. It can be observed that the estimated fault distance is 0.3540 km when the fault occurs in line section 9. The actual fault distance is 0.25km, and the percentage difference is approximately 20.8%.

In the next subsection, the overall performance of the proposed method is summarized in terms of ranking number and error measurement in the estimated fault impedance and fault distance values. Subsequently, the performance of the proposed algorithm will also be evaluated for varying fault inception angles, fault location and fault impedance values.

5.1 Ranking Performance Analysis

In this subsection, the overall performance in terms of ranking number is evaluated for all line sections with fault impedance values of 45, 55, 65, 75, 85 and 95 Ω. There are 35 line sections to be tested. All the faults are applied in the middle of line section with an inception angle of 90°. In this analysis, the accuracy of the proposed method is evaluated based on the total number of line sections with respect to the ranking number. Higher number of rank #1 indicates higher accuracy. Figure 12 shows the overall results for 35 line sections with six different HIF values. As shown in the figure, only 15 faulty line sections are successfully located in the first rank and one faulty line section falls in the fifth rank when the fault impedance value of 45Ω is applied. Besides that, a total number of 28 faulty line sections have been identified in rank #1 when the fault impedance value is 95 Ω and the rest can be located either in the second, third or fourth rank. In addition, it can be observed that the accuracy of the proposed faulted section identification algorithm increases as the fault impedance value is increased.

5.2 Analysis of Measurement Error

The performance of the proposed method is further evaluated in terms of error measurement of the fault impedance and fault distance values. In this case study, the fault impedance values of 45, 65 and 85 Ω are applied in the middle of line sections 9, 15, 23 and 33 with the fault inception angle of 90°. The results are shown in Table 4. As shown in the table, columns 3 and 6 represent the estimated fault impedance and fault distance values, respectively. Whereas columns 4 and 7 show the percentage of error for the fault impedance and fault distance values, respectively. The error calculation for fault impedance and fault distance values are shown in Eqs. (16) and (17), respectively.

$$\%\text{error} = \frac{|\text{Actual Value} - \text{Estimated Value}|}{\text{Actual Value}} \times 100\% \quad (16)$$

$$\%\text{error} = \frac{|\text{Actual Value} - \text{Estimated Value}|}{\text{Line Section}} \times 100\% \quad (17)$$

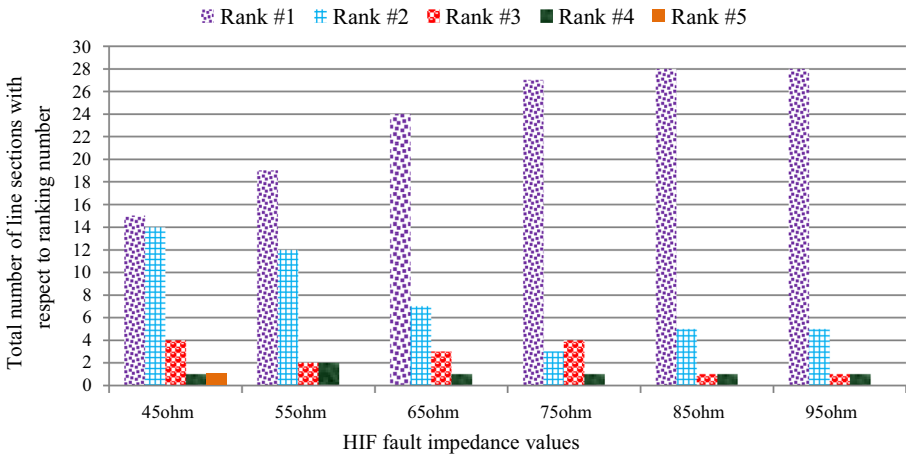

Fig. 12 Overall result for ranking analysis

Table 4 Analysis of measurement error

Fault impedance (Ω)	Faulty section	Estimated fault impedance (Ω)	% error	Fault distance (km)	Estimated fault distance (km)	% error
45Ω	9	44.86	0.32%	0.2500	0.3540	20.80%
	15	44.87	0.29%	0.2500	0.3554	21.08%
	23	44.37	1.41%	0.0500	0.0865	36.48%
	33	45.39	0.87%	0.6500	0.7249	5.76%
65Ω	9	64.98	0.03%	0.2500	0.3117	12.34%
	15	64.96	0.05%	0.2500	0.3175	13.50%
	23	64.68	0.49%	0.0500	0.0724	22.36%
	33	65.36	0.56%	0.6500	0.6769	2.07%
85Ω	9	85.17	0.19%	0.2500	0.2682	3.65%
	15	84.97	0.04%	0.2500	0.3040	10.79%
	23	84.63	0.43%	0.0500	0.0712	21.16%
	33	85.46	0.54%	0.6500	0.6012	3.76%

From the results, it can be observed that the fault impedance value can be estimated using the ANN technique with error below 1%, except for faulty section 23 with fault impedance value of 45Ω which yields a 1.41% error. There are also a few cases where the fault impedance value can be estimated to almost negligible error. These negligible error estimation is obtained when the fault impedance value is 65 Ω at line sections 9 and 15 as well as fault impedance value of 85 Ω at line section 15. In terms of estimated fault distance, there are a few cases where the algorithm can identify the fault location quite accurately with error below 6%. It must be noted that the rest of the fault distance cannot be located as precisely, but the errors remain below 40%. It also can be observed from the table that the error decreases as the fault impedance value increases for each line section.

Furthermore, the estimation error for increased number of case studies is analyzed here. The results of estimation error for 35 line sections and 6 different fault impedance values are shown in Fig. 13. The average estimation error for both fault impedance and fault distance values are represented by the blue and red dotted lines, respectively. It can be observed that the average error in estimating the fault impedance value remains below 0.42%, whereas the average estimation error for fault distance remains below 22%.

A calculation has been computed to obtain the maximum error in the fault distance estimation. Table 5 shows the accuracy range of the estimated fault distance for different fault impedance values. As can be observed in the table, when the fault impedance value increases, the range of the actual fault distance decreases such that the area to be inspected becomes smaller, thus expediting the restoration process and reducing the interruption time.

For instance, a fault occurs in the middle of line section 9 with fault impedance values of 45, 65 and 85 Ω, and the estimated fault distances are as shown in Table 4. The length of line section 9 is 0.5km, and the fault occurs at a point 0.25 km. Table 6 indicates the area to locate the fault becomes narrower as the fault impedance value increases.

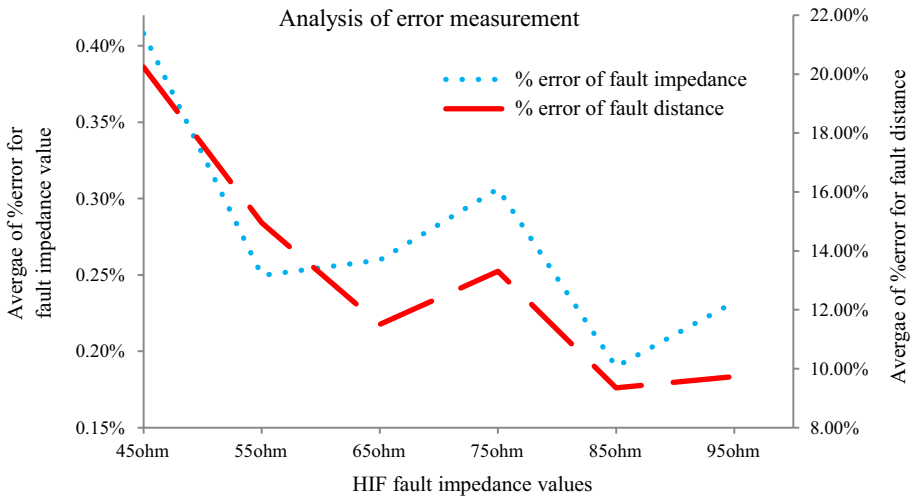

Fig. 13 Average of percentage error for measurement error analysis

Table 5 Range of actual fault distance

Fault impedance	Actual fault distance range
45 Ω	Estimated fault distance ± 37% of the line section length
55 Ω	Estimated fault distance ± 33% of the line section length
65 Ω	Estimated fault distance ± 26% of the line section length
75 Ω	Estimated fault distance ± 33% of the line section length
85 Ω	Estimated fault distance ± 22% of the line section length
95 Ω	Estimated fault distance ± 21% of the line section length

Table 6 Range of actual fault distance occurs at line section 9 (0.25 km)

	Estimated distance (km)	Actual distance range (km)	Range (km)
45 Ω	0.3540	0.3540 ± (37% × 0.5)	0.169–0.539
65 Ω	0.3117	0.3117 ± (26% × 0.5)	0.1817–0.4417
85 Ω	0.2682	0.2682 ± (22% × 0.5)	0.1582–0.3782

5.3 Variations of Fault Inception Angle

In this subsection, the effect of varying the fault inception angles is investigated to evaluate the reliability of the proposed algorithm. Five different fault inception angles comprising of 0°, 90°, 180°, 270° and 360° are analyzed and compared in terms of ranking number, estimated fault impedance and fault distance values. For this purpose, only four line sections are selected (line section 6, 15, 23 and 27) with different fault impedance values (45, 55, 85 and 95 Ω) applied in the middle of line section. The results of the analysis are shown in Table 7, and it can be observed that the proposed algorithm is capable of locating the faulty section, estimating the fault impedance and fault distance values to a satisfactory level. It also delivered the same ranking number when the fault inception angles are varied.

Table 7 Variation of inception angle

Fault impedance	Section	Inception angle (°)	Rank	Estimated fault impedance	Estimated fault distance
45 Ω	6	0	3	44.87	0.1394
		90	3	44.82	0.1433
		180	3	44.84	0.1420
		270	3	44.81	0.1435
		360	3	44.87	0.1394
55 Ω	15	0	2	55.10	0.3015
		90	2	55.06	0.3105
		180	2	55.09	0.3054
		270	2	55.05	0.3112
		360	2	55.10	0.3015
85 Ω	23	0	1	84.20	0.0861
		90	1	84.63	0.0712
		180	1	84.82	0.0648
		270	1	84.51	0.0754
		360	1	84.20	0.0861
95 Ω	27	0	1	94.63	0.4320
		90	1	95.06	0.3433
		180	1	95.20	0.3153
		270	1	94.97	0.3631
		360	1	94.63	0.4318

Table 8 45 Ω fault impedance value applied at different point in line sections 6, 15, 23 and 27

Section	Actual distance	Estimated fault value	Estimated fault distance	Ranking
6	0.0200	44.87	0.1233	2
	0.0500	44.84	0.1313	2
	0.1500	44.80	0.1550	3
	0.1800	44.79	0.1618	5
15	0.0500	44.82	0.2446	3
	0.1250	44.84	0.2862	1
	0.3750	44.84	0.4338	5
	0.4500	44.84	0.4767	5
23	0.0100	44.39	0.0826	1
	0.0250	44.38	0.0840	1
	0.0750	44.34	0.0892	1
	0.0900	44.33	0.0909	1
27	0.0594	44.77	0.3034	1
	0.1485	44.84	0.3443	1
	0.4455	44.97	0.4940	2
	0.5346	45.02	0.5353	4

Table 9 95 Ω fault impedance value applied at different point in line sections 6, 15, 23 and 27

Section	Actual distance	Estimated fault value	Estimated fault distance	Ranking
6	0.0200	95.14	0.0848	1
	0.0500	94.92	0.1077	1
	0.1500	94.93	0.1332	2
	0.1800	94.95	0.1399	2
15	0.0500	95.18	0.1268	3
	0.1250	95.22	0.1714	3
	0.3750	94.93	0.3892	4
	0.4500	94.95	0.4363	6
23	0.0100	94.90	0.0572	1
	0.0250	94.87	0.0601	1
	0.0750	94.73	0.0708	1
	0.0900	94.67	0.0745	1
27	0.0594	94.85	0.2398	3
	0.1485	94.91	0.2829	1
	0.4455	95.16	0.4117	2
	0.5346	95.14	0.4688	2

5.4 Variations of Fault Distance

Tables 8 and 9 show the results while 45 and 95 Ω fault impedance values are applied at different points in line sections 6, 15, 23 and 27, respectively. four different points in the line sections are represented by 10, 25, 75 and 90% of the line length. As shown in the tables, the fault impedance values can be successfully estimated with a very small error. It also delivered highly accurate results in faulty section ranking. There is only one case where the faulty section is identified in the 6 th rank when the fault impedance value of 95 Ω is applied at 90% of the line length of section 15. However, the fault distance cannot be identified as accurately, especially when the fault is applied at 10 and 25% of the line length. But, for those cases, the faulty section can be identified either at first, second or third rank. Therefore, it still can expedite the searching process of the fault location.

Table 10 Variation of fault impedance values applied in the middle of line section 23

Actual fault distance	Actual fault value	Estimated fault value	Estimated fault distance	Ranking
0.05	40	40.00	0.0555	3
	41	40.76	0.0681	1
	42	41.73	0.0721	1
	43	42.40	0.0854	1
	44	43.36	0.0871	1
	45	44.37	0.0865	1
	46	45.40	0.0836	4
	47	46.40	0.0810	6
	48	47.43	0.0761	6
	49	48.39	0.0729	4
	50	49.46	0.0648	4
	90	89.81	0.0512	2
	91	90.81	0.0649	1
	92	91.81	0.0660	1
	93	92.76	0.0680	1
	94	93.75	0.0679	1
	95	94.80	0.0652	1
	96	95.88	0.0611	3
	97	96.84	0.0602	5
	98	97.89	0.0558	3
	99	98.91	0.0519	2
	100	99.89	0.0487	2

5.5 Variations of Fault Impedance Value

The performance of the algorithm is further evaluated with the variation of fault impedance values applied in the middle of line section 23 and 27 as shown in Tables 10 and 11. The fault impedance values vary from 40–50 and 90–100 Ω in increment of 1 Ω. As shown in Tables 10 and 11, the fault impedance values are successfully estimated with small errors. However, the fault distance cannot be estimated

Table 11 Variation of fault impedance values applied in the middle of line section 27

Actual fault distance	Actual fault value	Estimated fault value	Estimated fault distance	Ranking
0.297	40	40.00	0.5175	1
	41	40.85	0.5361	1
	42	41.89	0.5117	1
	43	42.94	0.4778	1
	44	43.91	0.4535	1
	45	44.89	0.4235	2
	46	45.91	0.3777	4
	47	46.97	0.3216	2
	48	47.86	0.2929	3
	49	48.90	0.2311	2
	50	49.94	0.1638	2
	90	90.00	0.1383	2
	91	91.04	0.4699	1
	92	92.03	0.4453	1
	93	93.02	0.4177	1
	94	93.97	0.3953	1
	95	95.06	0.3433	1
	96	96.09	0.2993	2
	97	97.07	0.2623	4
	98	98.04	0.2247	2
	99	98.99	0.1885	2
	100	99.78	0.1818	2

as accurately as well. But the identification of the fault location is assisted with satisfactory faulty section ranking. Based on the results, all the faulty sections can be identified within the 6th rank. Therefore, the fault localization and restoration process can also be expedited when the fault impedance values are varied.

5.6 Comparing the Proposed Method to Other Similar Methods

Table 12 shows the comparison of the proposed method with the results from other presented papers [3,9,10,12,21,26]. Each of these papers have their own advantages and disadvantages. One of the comparison is based on the percentage of error for fault location. The percentage of error is calculated as follows:

$$\text{Error}\% = \frac{|\text{Actual\_location} - \text{Estimated\_location}|}{\text{Total\_cable\_length}} \times 100\% \quad (18)$$

The maximum percentage of fault location error for each method is shown in Table 12. In this proposed method the maximum percentage of error shown in Table 12 is 2.37%. This maximum fault location error is recorded when the fault occurred along the line section 27 with fault impedance of 45 Ω. It is noted that even though the percentage error is quite high, but the rank for that particular faulty section is #1. Therefore, the fault location can be identified immediately.

Besides that, in this proposed method the fault impedance can be estimated accurately, which the other presented papers do not analyze. The maximum error obtained between the estimated and actual fault impedance is 0.8 Ω when a fault is applied in Line Section 23 with the inception angle of 0° and 360° while the fault impedance is 85 Ω as shown in Table 7. The estimated fault impedance is 84.20 Ω whereas the actual fault impedance is 85 Ω.

It is observed that the percentage error of fault location for this proposed method is higher than the other presented papers. But, all required important information such as fault impedance, fault distance and faulty section are provided which are salient advantages of this proposed method. Besides that, the actual fault location can be identified easily with higher accuracy of faulty section.

Table 12 Comparing the proposed method to other similar methods

Technique used in other similar paper	Type of results presented by each of the techniques				
	Determination of fault type	Estimate the fault impedance	Estimate the fault distance	Identify the faulty section	%Error of fault location
Modal analysis[3]	–	–	X	X	<0.83%
Wavelet, SVR[9]	–	–	X	–	<1.43%
Wavelet, ANN, FLS[10]	X	–	X	–	<1.5%
EMD, CVR[12]	–	–	X	–	<0.67%
Unsynchronizedphasor[21]	–	–	X	X	<0.854%
Wavelet[26]	X	–	–	X	–
Proposed method in this paper	–	X	X	X	<2.37%

X—the technique presented the results
— the technique does not presented the results

6 Conclusion

In this paper, a new HIF location technique for an underground distribution network is presented. The measured three-phase voltage and current waveforms are first decomposed using DWT to obtain the energy values of the approximation coefficients. Then the energy values are used as an inputs to the ANN to estimate the fault impedance value. This is followed by the application of database approach to locate the potential faulty sections through the SD score computations. Finally, the fault distance is calculated.

The performance of the proposed algorithm in localizing simulated SLGF in a distribution network is tested. The results showed that the proposed algorithm managed to estimate the fault impedance value with an average percentage error less than 0.42%. The fault distance is also estimated to a satisfactory level with an average percentage error less than 2.37%. In addition, the algorithm has been demonstrated to deliver convincing results even under varied fault inception angles. In conclusion, the proposed method can be used to facilitate a speedy fault location and supply restoration process. In future work, different types of artificial intelligence methods can be tested to improve the accuracy of the proposed method. Hybrid techniques consisting of two or more artificial intelligence methods can also be investigated.

References

1. Filomena, A.D.; et al.: Fault location for underground distribution feeders: an extended impedance-based formulation with capacitive current compensation. Int. J. Electr. Power Energy Syst. **31**, 489–496 (2009)
2. Board, I.-S.S.; et al.: IEEE Guide for Determining Fault Location on AC Transmission and Distribution Lines. Institute of Electrical and Electronics Engineers, New York (2005)
3. Sadeh, J.; et al.: A new fault location algorithm for radial distribution systems using modal analysis. Int. J. Electr. Power Energy Syst. **45**, 271–278 (2013)
4. Thukaram, D.; et al.: Artificial neural network and support vector machine approach for locating faults in radial distribution systems. IEEE Trans. Power Deliv. **20**, 710–721 (2005)
5. Moshtagh, J.; Aggarwal, R.K.: A new approach to ungrounded fault location in a three-phase underground distribution system using combined neural networks & wavelet analysis. In: Canadian Conference on Electrical and Computer Engineering, CCECE '06, pp. 376–381 (2006)
6. Elhaffar, A.M.: Power Transmission Line Fault Location Based on Current Traveling Waves. Faculty of Electronics, Communications and Automation, Helsinki University of Technology, Degree of Doctor of Science in Technology, ESPoo (2008)
7. Borghetti, A.; et al.: Continuous-wavelet transform for fault location in distribution power networks: definition of mother wavelets inferred from fault originated transients. IEEE Trans. Power Syst. **23**, 380–388 (2008)
8. Pourahmadi-Nakhli, M.; Safavi, A.A.: Path characteristic frequency-based fault locating in radial distribution systems using wavelets and neural networks. IEEE Trans. Power Deliv. **26**, 772–781 (2011)
9. Ye, L.; et al.: An improved fault-location method for distribution system using wavelets and support vector regression. Int. J. Electr. Power Energy Syst. **55**, 467–472 (2014)
10. Rafinia, A.; Moshtagh, J.: A new approach to fault location in three-phase underground distribution system using combination of wavelet analysis with ANN and FLS. Int. J. Electr. Power Energy Syst. **55**, 261–274 (2014)
11. Chunju, F.; et al.: Application of wavelet fuzzy neural network in locating single line to ground fault (SLG) in distribution lines. Int. J. Electr. Power Energy Syst. **29**, 497–503 (2007)
12. Khorramdel, B.; et al.: Fault locating in large distribution systems by empirical mode decomposition and core vector regression. Int. J. Electr. Power Energy Syst. **58**, 215–225 (2014)
13. Zayandehroodi, H.; et al.: A novel neural network and backtracking based protection coordination scheme for distribution system with distributed generation. Int. J. Electr. Power Energy Syst. **43**, 868–879 (2012)
14. Girgis, A.A.; et al.: A new fault location technique for two- and three-terminal lines. IEEE Trans. Power Deliv. **7**, 98–107 (1992)
15. Novosel, D.; et al.: System for locating faults and estimating fault resistance in distribution networks with tapped loads. Google Patents (1998)
16. Liang, R.; et al.: Fault location based on single terminal travelling wave analysis in radial distribution network. Int. J. Electr. Power Energy Syst. **66**, 160–165 (2015)
17. Aslan, Y.; Yağan, Y.E.: Artificial neural-network-based fault location for power distribution lines using the frequency spectra of fault data. In: Electrical Engineering, pp. 1–11 (2016)
18. Borghetti, A.; et al.: On the use of continuous-wavelet transform for fault location in distribution power systems. Int. J. Electr. Power Energy Syst. **28**, 608–617 (2006)
19. Goudarzi, M.; et al.: Improved fault location algorithm for radial distribution systems with discrete and continuous wavelet analysis. Int. J. Electr. Power Energy Syst. **67**, 423–430 (2015)
20. Prabhavathi, D.; et al.: Detection and location of faults in three-phase 11 kv underground power cables by discrete wavelet transform. In: Singh R.; Choudhury, S.(eds.) Proceeding of International Conference on Intelligent Communication, Control and Devices : ICICCD 2016, pp. 113–125. Springer, Singapore (2017)
21. Nam, S.-R.; et al.: Single line-to-ground fault location based on unsynchronized phasors in automated ungrounded distribution systems. Electr. Power Syst. Res. **86**, 151–157 (2012)
22. Xiu, W.; Liao, Y.: Novel fault location methods for ungrounded radial distribution systems using measurements at substation. Electr. Power Syst. Res. **106**, 95–100 (2014)
23. Iurinic, L.; et al.: Distribution systems high impedance fault location: a parameter estimation approach. IEEE Trans. Power Deliv. **31**, 1806–1814 (2015)
24. https://hvdc.ca/pscad/.
25. Mathworks. Neural Network Toolbox. In: Training Functions, Mathwork, Inc., 2016. https://www.mathworks.com/products/neural-network.html (2016)
26. Bakar, A.H.A.; et al.: High impedance fault location in 11 kV underground distribution systems using wavelet transforms. Int. J. Electr. Power Energy Syst. **55**, 723–730 (2014)